

Electronic structure of yttrium oxide

F. Jollet, C. Noguera,* N. Thromat, M. Gautier, and J. P. Duraud

Centre d'Etudes Nucléaires de Saclay, Département de Physique Générale/Service de Physique des Atomes et des surfaces (DPhG/SPAS), Bâtiment 125, 91191 Gif-sur-Yvette, France

(Received 21 November 1989; revised manuscript received 17 April 1990)

The electronic structure of stoichiometric Y_2O_3 is studied both theoretically and experimentally. X-ray absorption, performed through total-yield measurements at the K and L_{II} edges of yttrium atoms and the K edge of oxygen atoms, through total-yield measurements has given access to empty states of various orbital characters in the conduction band. The shape of the valence band was obtained by means of photoemission spectroscopy. These results are compared with self-consistent, semiempirical tight-binding calculations applied to clusters of increasing sizes, which lead to local densities of states. We show that the quasi-octahedral local environment of the yttrium atoms is responsible for the splitting of their d levels. However, this ligand-field approach is not sufficient to account for the yttrium and oxygen K thresholds, nor for the shape of the valence band for which band effects are important. The two-peak structure of the oxygen K edge results from the hybridization of the O p orbitals with the e_g and t_{1u} states on the yttrium atoms. Three peaks are detected in the valence band: We show that they suggest the existence of direct-hopping terms between neighboring oxygen atoms. Finally, the various calculations have given an estimate of the degree of covalency of the Y—O bond.

I. INTRODUCTION

Yttrium oxide is a highly refractory material ($T_f \approx 2410^\circ\text{C}$) which presents a good chemical stability, a high resistivity, and a high breakdown strength. Its technological interest is widely developing. Apart from its well-known use in ceramic processing (zirconia stabilization), Y_2O_3 is a promising material as a substrate for superconductive thin films. Y_2O_3 crystals have received much attention as a host of the rare-earth-doped laser.¹ Moreover, its high dielectric constant ($\epsilon_0 = 14-17$) makes Y_2O_3 a possible candidate for silicon very-large-scale-integration applications.²

However, the properties of Y_2O_3 are strongly dependent upon the presence of defects. These latter are known³ to modify the electrical conductivity. In a recent work⁴ we showed that oxygen deficiency induces important changes in the mechanical properties (decrease of the fracture toughness). In addition, an increase of the surface conductivity was noticed after an exposure to an ionizing beam.⁵ In order to reach the microscopic origin of such changes, the evolution of the Y—O bond was studied by means of Auger and photoelectron spectroscopy as a function of the concentration of oxygen vacancies: an increase in the covalent character of the bonding was found.^{6,7}

Yet a deeper insight into the role of oxygen vacancies requires a better knowledge of the electronic structure of "perfect" Y_2O_3 . Strangely enough, only a few studies have been devoted to this topic. A value of about 5.5 eV for the energy gap was measured by thermal electronic emission⁸ and optical vuv spectroscopy.⁹ Electron-energy-loss spectroscopy in the transmission mode brought information on the yttrium L_I and $L_{II,III}$ edges and on the oxygen K edge.^{10,11} From a theoretical point

of view, only one density-of-states (DOS) calculation was performed on a cluster of nine atoms, which is far too small to account for all crystal symmetries and for a correct hybridization of orbitals.¹² To our knowledge, no band structure is available due to the large number of atoms in the unit cell. It is the purpose of this paper to give a full description of the electronic structure of perfect Y_2O_3 , on the basis of both an experimental and a theoretical approach. The experimental part, described in Sec. II, makes use of x-ray photoemission spectroscopy (XPS), which yields the total DOS in the valence band, and of x-ray absorption at the yttrium K and L_{II} edges and at the oxygen K edge, which are related to local DOS in the conduction band around each atom, projected on given orbital momenta. The results are presented in Sec. III and a first discussion in the frame of a ligand-field approach is sketched. In order to go further into the interpretation of these results, we performed a DOS calculation on clusters of increasing sizes, using a semiempirical tight-binding method. Such a method was chosen for Y_2O_3 since electronic correlations are not expected to be dominant. Section IV is devoted to the description of the method and to a discussion of the total and partial DOS, as well as of the ionic charges on Y and O atoms. The comparison with the experimental results stresses the importance of band effects, beyond the ligand-field approach.

II. EXPERIMENT

A. Instrumentation

X-ray-absorption spectroscopy (XAS) experiments were carried out on the SA7, SU7, and D4 beam lines at the super-ACO and DCI synchrotron radiation facilities [Laboratoire pour l'Utilisation du Rayonnement

Electromagnétique (LURE), Orsay]. The corresponding monochromators were as follows.

A “two-parallel crystal” type (InSb), whose diffracting surfaces are cut parallel to the (111) plane, allowing a photon energy range from 1.5 to 2.5 keV, on the SA7 beam line.

A Si crystal, the orientation of which is giving an energy varying from 400 to 800 eV on the SU7 line.

A “channel-cut” Si crystal, whose diffracting surfaces are cut parallel to the (220) plane: the energy range obtained was 6–30 keV using first-order diffraction for the D4 line of DCI.

The primary photon beam intensity I_0 was monitored thanks to an ionization chamber while the total electron current $I_S(E)$ was recorded as a function of the photon energy E thanks to a Channeltron (Galileo). The total yield includes elastic and inelastic or secondary Auger electrons, photoelectrons, and the secondary electrons produced by the latter. It was shown¹³ that in the extended x-ray-absorption fine-structure (EXAFS) region

$$\nu = I_S(E)/I_0 = \mu_0(E)f(E)[1 + \chi(E)R(E)], \quad (1)$$

where $\mu_0(E)$ is the atomic absorption coefficient, $f(E)$ is a slowly varying function of E . $R(E)$ is close to unity near threshold and decreases very slowly at higher energy; finally $\chi(E)$ is the EXAFS function which represents the elastic collisions of the photoelectron on neighboring atoms. The total electron yield thus follows closely the shape of the absorption coefficient

$$\mu(E) = \mu_0(E)[1 + \chi(E)] \quad (2)$$

in this energy range. Near the absorption edge, multiple-scattering events must be taken into account so that we cannot use the EXAFS function. However, it has been experimentally established that the total electron yield measurements led to the same shape for thresholds as the x-ray-absorption measurements.^{14–16}

Photoemission experiments were performed in a VG Instruments, Inc., Escalab Mark II with a base pressure around 5×10^{-11} mbar. XPS spectra were recorded using a monochromatized x-ray source with an aluminum anode ($h\nu = 1486.6$ eV). Emitted electrons were filtered in energy in a hemispherical analyzer, which, operated in the constant analyzer energy mode, gave $N(E_K)$ curves (the number of electrons as a function of their kinetic energy E_K). The pass energy was adjusted between 10 and 30 eV for XPS. At these energies, the analyzer broadening was 0.8 eV. Calibration of the spectrometer was performed using the Au $4f_{7/2}$ line, the binding energy of which is 84 eV. A detection was made by counting; the data were stored and processed on a microcomputer. In order to overcome sample charging under the radiation beam, an electron flood gun was used (LEG 51, 0.5 eV, 200 μ A) so as to obtain the Y $3d_{5/2}$ photoemission line at the binding energy 160.6 eV, characteristic of Y_2O_3 .

B. Samples

Pure Y_2O_3 (99.999% purity, Rhône-Poulenc, France) powders were sintered under hot isostatic pressure (HIP):

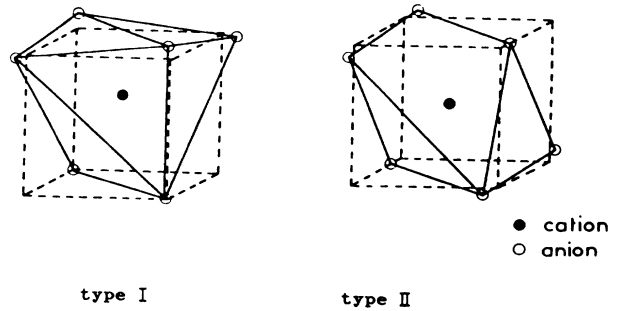


FIG. 1. Quasi-octahedral site of type-I and type-II yttrium atoms.

150 MPa at 1450 °C for 45 min. After HIP processing, samples of thickness 1 mm were cut and mechanically polished, then annealed for 2 h at 1500 °C in air, to remove the intrinsic oxygen vacancies and the residual stresses resulting from the sintering process. Some of the samples were coated with a 30-Å-thick carbon layer, in order to check the influence of surface charging on the XAS data.

X-ray diffraction and EXAFS measurements (at the yttrium K edge in the transmission mode)⁷ confirmed that the crystallographic structure, characteristic of Y_2O_3 , was achieved, i.e., C -type rare-earth sesquioxide structure [space group $T_h^7 (Ia\bar{3})$], closely related to the fluorite structure with a cell parameter $a = 10.604$ Å. In the fluorite lattice, each cation is surrounded by eight anions located at the corners of a cube. The C -type structure is derived by removing one-quarter of the anions and slightly rearranging the remaining ones. For 75% of the cations (called type I in the following) the vacancies lie at the ends of a face diagonal, while for the 25% others (called type II), they lie at the ends of a body diagonal. The real positions of the atoms are slightly shifted from the cube corners. Each yttrium atom occupies a strongly distorted octahedral site, as schematically depicted in Fig. 1: its first oxygen neighbors lie at a mean distance of 2.29 Å; the second coordination shell consists of 12 yttrium atoms at 3.75 Å, and a third one of 18 oxygen atoms at 4.39 Å (mean distances). Each oxygen atom is in a slightly distorted tetrahedral site: its first neighbors are three type-I and one type-II yttrium atoms: the second coordination shell is made of four oxygen atoms at 2.65 Å and the third one of nine oxygen atoms at 3.75 Å.

III. RESULTS AND DISCUSSION

A. X-ray absorption

1. General features

Figures 2 and 3 represent, respectively, x-ray-absorption spectra at the K and L_{II} edges of yttrium. Intense white lines due to dipolar transitions of the $s \rightarrow p$ or $p \rightarrow d$ type are observed. Beyond the ranges of the figures, EXAFS oscillations were clearly visible and were used⁷ to get information on the local structure, as mentioned in Sec. II B. The oxygen K edge appears more

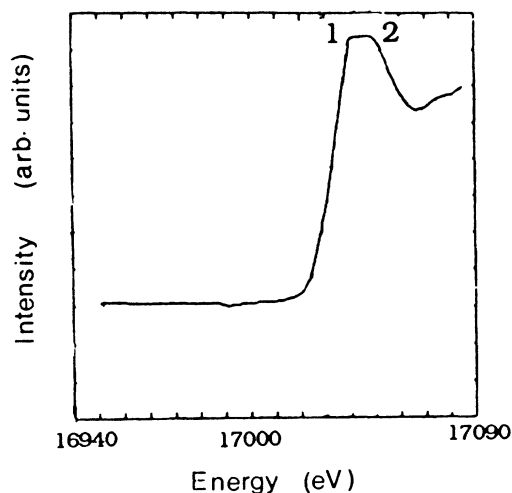


FIG. 2. Y K absorption threshold in Y_2O_3 .

complex, as may be inferred from a comparison between Fig. 4(a) obtained on a stoichiometric sample (prepared as explained in Sec. II B), and Fig. 4(b) which corresponds to a nonstoichiometric sample, heated under vacuum (1700°C ; $P=10^{-6}$ mbar) for 2 h. For this latter sample, EXAFS results showed that 10% of the oxygen atoms were removed from the lattice. We noticed that the sample was more conductive, and consequently, no charging effect was observed under either electron or x-ray bombardment, contrary to the stoichiometric one. It seems likely that charging-up, occurring at a microscopic level on the stoichiometric sample, hampers an accurate observation of the oxygen K edge: when a hole is created on an oxygen atom, it may deexcite, giving an oxygen atom displacement,¹⁷ the more so as the natural vacancies of the lattice may receive an interstitial oxygen atom. These point defects then create traps in the gap and charging-up may occur. The following remarks reinforce this point. (i) No EXAFS oscillations could be seen above the oxygen K edge on the stoichiometric sample, whereas they clearly appear on the reduced one. (ii) The oxygen K edge of reduced Y_2O_3 [Fig. 4(b)] presents a great similarity with that of pure Y_2O_3 obtained from electron-

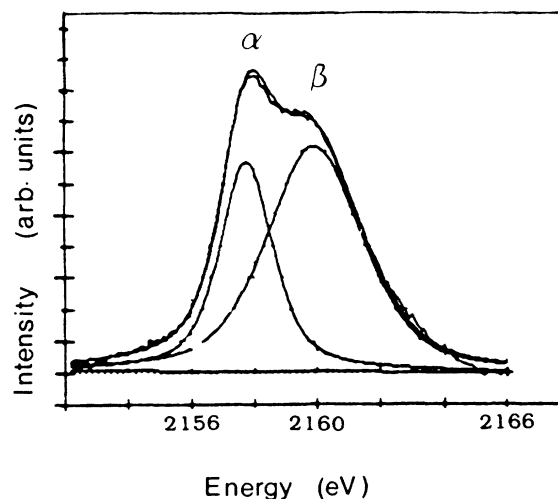


FIG. 3. Y L_{II} absorption threshold in Y_2O_3 after subtraction of background and decomposition into Gaussians.

energy-loss-spectroscopy (EELS) measurements.¹¹ (iii) The same shape was obtained for samples having different concentrations of oxygen vacancies. Consequently, in the following, we will rather compare our calculations with the spectrum of Fig. 4(b).

2. Threshold energies

The three absorption spectra (Figs. 2–4) exhibit very intense structures, with steep slopes on their low-energy sides and no superimposed shoulders. Therefore, the threshold positions can be safely defined as the inflection point of the first intense peak.

A precise comparison between binding energies obtained by XAS and XPS requires one to take into account the many-body relaxation effects following the creation of the core hole. These are distinct in the two spectroscopic modes. In XAS, the excitation electron is promoted to a vacant state at the bottom of the conduction band; therefore the core hole is (at least partially) screened by the photoelectron. On the other hand, in XPS, the excited electron is ejected far above the Fermi level with a large

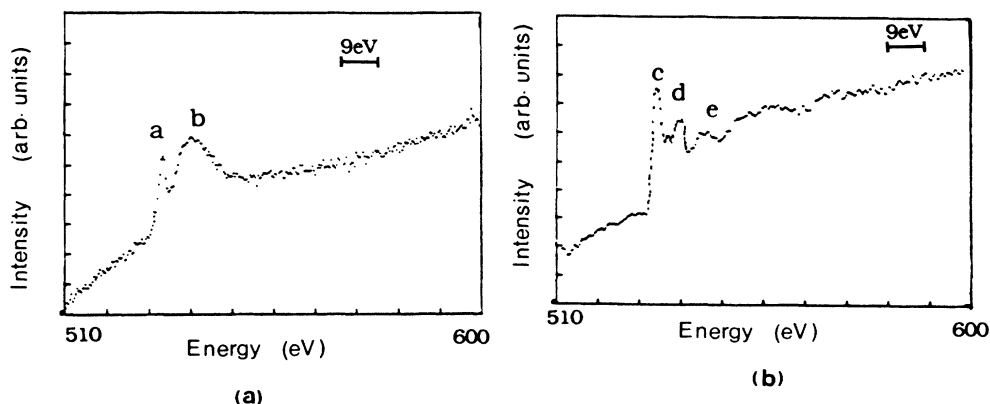


FIG. 4. O K absorption threshold in (a) stoichiometric Y_2O_3 and in (b) reduced Y_2O_3 .

kinetic energy (955 eV in the case of the oxygen 1s level); the only contribution to the screening comes from valence electrons, but these processes are not very efficient in insulating materials. Quite generally, the XPS binding energy may be written as

$$E_b = |\varepsilon| - E_R^{\text{XPS}}, \quad (3)$$

where ε is the mono-electronic orbital energy referred to the Fermi level and E_R^{XPS} the XPS relaxation energy. Similarly, the XAS edge energy reads

$$E_{\text{edge}} = |\varepsilon| - E_R^{\text{XAS}} + \alpha E_g, \quad (4)$$

where E_g is the band-gap width and E_R^{XAS} the XAS relaxation energy. The position of the Fermi level in the gap is indicated by ($0 < \alpha < 1$). The preceding discussion suggests that $E_R^{\text{XAS}} > E_R^{\text{XPS}}$.

This is indeed what we find when a 1s electron of an oxygen atom is excited in Y_2O_3 : we determine experimentally $E_{\text{edge}} = 531$ eV and $E_b = 531$ eV. Equations (3) and (4) lead to $E_R^{\text{XAS}} - E_R^{\text{XPS}} = \alpha E_g$ around an oxygen 1s core hole, whatever the value of α may be.

We also find that the inequality $E_R^{\text{XAS}} > E_R^{\text{XPS}}$ is valid around an yttrium core hole. A direct comparison between XPS and XAS binding energies was not possible for the yttrium K or L_{II} levels which are too energetic to be excited by our conventional x-ray sources. However, by comparing the XAS binding energy in the metal and in the oxide, one can measure an XAS chemical shift, in close analogy with the XPS one. This point has been extensively discussed in EELS spectroscopy in which the final states are similar to those reached in XAS,¹⁸ and in which it was argued that an EELS relaxation energy smaller than the XPS one was responsible for a smaller EELS chemical shift. One can write

$$\begin{aligned} \Delta^{\text{XAS}} &= E_{\text{edge}}(\text{oxide}) - E_{\text{edge}}(\text{metal}) \\ &= |\varepsilon(\text{oxide})| - |\varepsilon(\text{metal})| - E_R^{\text{XAS}}(\text{oxide}) \\ &\quad + E_R^{\text{XAS}}(\text{metal}) + \alpha E_g, \end{aligned} \quad (5)$$

$$\begin{aligned} \Delta^{\text{XPS}} &= E_b(\text{oxide}) - E_b(\text{metal}) \\ &= |\varepsilon(\text{oxide})| - |\varepsilon(\text{metal})| - E_R^{\text{XPS}}(\text{oxide}) \\ &\quad + E_R^{\text{XPS}}(\text{metal}), \end{aligned} \quad (6)$$

since in a metal $E_R^{\text{XAS}}(\text{metal}) = E_R^{\text{XPS}}(\text{metal})$ because the conduction electrons always provide a perfect screening:

$$\Delta^{\text{XPS}} - \Delta^{\text{XAS}} = E_R^{\text{XAS}}(\text{oxide}) - E_R^{\text{XPS}}(\text{oxide}) - \alpha E_g. \quad (7)$$

In the case of the K edge of yttrium, we find $E_{\text{edge}}(\text{oxide}) = 17049$ eV and $E_{\text{edge}}(\text{metal}) = 17046$ eV in agreement with Ref. 19. Consequently $\Delta^{\text{XAS}} = 3$ eV. An XPS chemical shift of 3 eV was obtained on the yttrium $3d$ levels²⁰ which can be excited by the conventional x-ray source. As a first approximation it can be considered²¹ that the chemical shifts of different core levels on the same atom differ only by a few tenths of eV. For the yttrium L_{II} edge, we will thus take $\Delta^{\text{XPS}} \approx 3$ eV. From (7) we conclude that

$$E_R^{\text{XAS}}(\text{oxide}) - E_R^{\text{XPS}}(\text{oxide}) \approx \alpha E_g$$

around an yttrium core hole.

For Y_2O_3 , we thus find that $E_R^{\text{XAS}} - E_R^{\text{XPS}}$ has the same magnitude whether the hole is created on an yttrium atom or on an oxygen atom. To our knowledge, there is no such comparison for other oxides in the literature, so that it is not possible at the present time to deduce any general law.

3. Fine structures near threshold

a. The yttrium K edge. The XAS spectrum displays two structures labeled 1 and 2 in Fig. 2, separated by about 5 eV. The intrinsic width of the K level [≈ 4 eV (Ref. 12)] and the experimental broadening hamper a better resolution.

b. The yttrium L_{II} edge. The L_{II} edge is clearly splitting into two components, labeled α and β in Fig. 3, separated by 2.16 eV. (In this case the intrinsic width of the L_{II} level is only 2 eV.²²) This shape is characteristic of the L_{II} edges of transition-metal oxides in which the cation occupies an octahedral site, and can be understood by a ligand-field theory, reasonable in systems in which the electronic states are well localized. The octahedral environment of the yttrium atoms, due to their six oxygen neighbors, splits the unoccupied d levels into t_{2g} and e_g molecular orbitals (respectively, at lower and higher energies), which are final states for a dipolar transition starting from the yttrium L_{II} level.

c. The oxygen K edge. At least three structures are clearly observed in Fig. 4(b), labeled $c-e$. This is in good agreement with previous EELS results obtained at the oxygen K edge of rare-earth oxides.²³ This shape was considered to be a fingerprint of a tetrahedral environment for the oxygen atoms. We will present in Sec. IV an interpretation of these structures based on density-of-states calculations.

The energy positions of the various fine structures observed in the XAS spectra are summarized in Table I; they are referenced from the absorption thresholds.

B. Photoelectron spectroscopy

Figure 5 represents the valence-band spectra obtained with the Al K_α photon source: the valence band displays three structures labeled I, II, and III, the interpretation of which will be discussed in Sec. IV.

TABLE I. Summary of the various fine structure observed in the XAS spectra, referenced from the absorption thresholds.

Threshold	Y K		Y L_{II}		O K (b)		
Structure	1	2	α	β	c	d	e
Energy (eV)	10.45	16.17	1.3	2.9	1	6	11

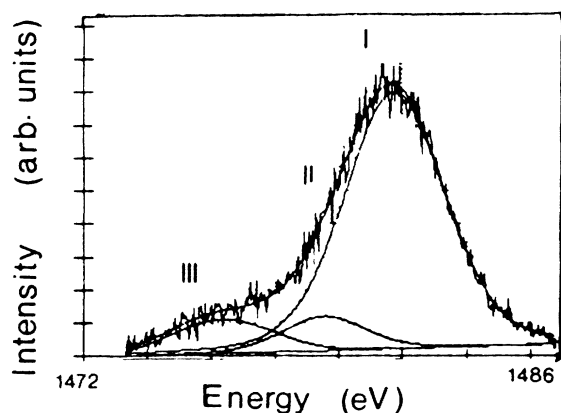


FIG. 5. Y_2O_3 valence band determined by XPS Al $K\alpha$ after subtraction of background and decomposition in Gaussians.

IV. DENSITY-OF-STATES CALCULATIONS

In order to interpret our experimental results, we have performed semiempirical tight-binding calculations²⁴ on clusters of increasing size. Such an approach is known to give good results for semiconductors²⁵ and is expected to be well suited to insulating oxides in the absence of strong electronic correlations.

A. The method

The eigenstates of the system are developed on an orthogonal basis of atomic orbitals including $2s$ and $2p$ orbitals for the oxygen atoms; $4d$, $5s$, and $5p$ orbitals for the yttrium atoms. This limited basis is adequate for reproducing structures in the lower part of the conduction band on which we focus in this paper. The study of more remote x-ray-absorption near-edge structure features would require a larger basis. The off-diagonal matrix elements, corresponding to hopping between neighboring atoms are evaluated thanks to Harrison's empirical formula;²⁴ when explicitly specified, second-neighbor oxygen-oxygen hopping terms were also added, as was done in SiO_2 by Allan *et al.*²⁶ The diagonal-matrix elements include the orbital energies, tabulated in Table II, corrected by intra-atomic Coulomb terms, evaluated in the Hartree approximation. These corrections require the knowledge of the number of electrons on each ion, which is an output of the calculation. A self-consistent procedure is thus necessary, especially in ionic systems where a large charge transfer between anions and cations occurs. The values of the intra-atomic interactions on each kind of atoms should be chosen so as to reproduce both the value of the band gap and of the dielectric constant at the zone boundary. In this work, we have only

TABLE II. Orbital energies used for the semiempirical tight-binding calculations.

Orbital	s (eV)	p (eV)	d (eV)
Oxygen	-29.14	-14.3	
Yttrium	-4.95	-2.86	-4.92

checked that the first condition was fulfilled.

The tight-binding method is very flexible and allows an easy projection of the DOS on particular sites and/or particular angular momenta. In addition, it yields the value of the band gap and the importance of the charge transfer.

We have computed the electronic structure of clusters of the largest possible size. We noticed that only the atoms close to the center of the cluster present a reliable DOS. For the outer ones, which have not their complete environment, "surface effects" occur, including shifts of energy and narrowing of bands. As a consequence we choose clusters centered on an yttrium atom (called Y clusters in the following) whenever the conduction band or yttrium thresholds are concerned, while clusters centered on an oxygen atom (called O clusters) are better suited to the study of the valence band or oxygen thresholds. In both cases, only the local DOS on the central atom is discussed.

Unfortunately, we were not able to reach large enough sizes to be sure that the DOS on the central atom was free from "surface" effects. We used Y clusters of 55 atoms and O clusters of 45 atoms. This is less than the number of atoms in the unit cell, which includes 32 yttrium atoms and 48 oxygen atoms, but still presents a progress compared with the existing calculation on a nine-atom cluster.¹² In the case of Y clusters, the successive shells contain 6 oxygen, 12 yttrium, and 36 oxygen atoms. The central oxygen atom in an O cluster is surrounded by 4 yttrium atoms in the first shell, 16 oxygen atoms in the second one, and 24 yttrium atoms in the third one.

We noticed that, in order to be able to reach self-consistency, the atoms in the next to last shell had to be surrounded by all their first neighbors. This gives a severe restriction on how to build the cluster, in the absence of which a metallic surface might be produced, yielding a breakdown of the self-consistent procedure. A direct consequence of this requirement is the non-neutrality of our clusters: their global charge was obtained by formally affecting eight valence electrons to each oxygen ion and zero to the yttrium one.

Since the structure includes two inequivalent yttrium sites (type I and type II as discussed in Sec. II B), two kinds of Y clusters were also considered, labeled I and II in the following. Their DOS were weighted, respectively, by $\frac{3}{4}$ and $\frac{1}{4}$ to get the mean local DOS. In order to obtain a continuous DOS, the eigenstate energies have been convoluted with a 0.9 eV wide Gaussian-type function, which approximately corresponds to the experimental broadening.

B. Local DOS on the yttrium atoms

We have calculated the electronic structure of type-I and type-II Y clusters and in this section we examine successively their p and d projections, in connection with the observed K and L_{II} yttrium edges.

1. K edge

The p empty states on the yttrium atoms represent the final states of a dipolar transition from the $1s$ atomic lev-

el. Figure 6 displays the p local DOS for type-I and type-II clusters and their mean value. Two structures a and b , distant by about 1.5 eV, are clearly distinguished, together with three other weaker structures. These latter seem to be related to finite-size effects which include different Coulomb fields on yttrium atoms in different shells: we will discard them in the following. The two stronger peaks are interpreted as due to a lifting of degeneracy of the p orbitals in the distorted octahedral site, together with longer-range hybridization effects (quantum interferences with similar states on other yttrium atoms, which are not present in a ligand-field approach, and that we will call band effects in the following). Actually, in a perfect octahedral environment, the three p orbitals are degenerated. But we saw in Sec. II B that the environment is far from being perfect due to the location of the oxygen atoms on the cube vertices and due to the occurrence of various Y-O first-neighbor distances. The first effect yields a clear splitting of the p peak, especially in type-II clusters, while the second one erases part of this separation. The calculation that we have done on a seven-atom cluster showed that most of the dedoubling comes from band effects rather than from local-field effects.

Yet the 1.5 eV energy difference between peaks a and b is too small compared with the experimental one (≈ 5 eV), indicating a possible existence of direct Y-Y hopping terms that would reinforce the band effects. We have not tried to introduce these terms, because this would increase the number of unknown empirical parameters.

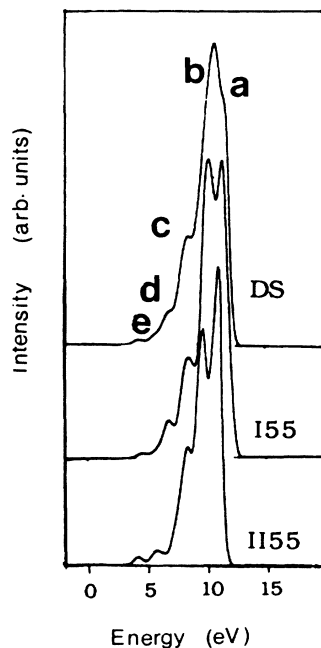


FIG. 6. p local DOS (conduction band) on type-I and type-II yttrium atoms, at the center of a 55-atom cluster (I55 and II55); mean value (DS). Peaks a and b correspond to the experimental peaks 1 and 2 of Fig. 2. The peaks c – e are due to finite-size effects (see text).

2. L_{II} edge

The excitation of an electron from a $2p$ state leads mainly to unoccupied d states. Figure 7 displays the projection of the local DOS on d orbitals for the two cluster types. Two structures are clearly distinguished, separated by 2.2 eV, in agreement with the experimental result. We attribute them to the splitting of the d states in an octahedral site, into e_g (peak g) and t_{2g} (peak f) components, slightly modified by local distortion and band effects. This statement may be checked on clusters of seven atoms, as depicted in Fig. 8: the perfect octahedral environment is characterized by the two e_g and t_{2g} peaks, with intensities in the ratio 2:3, while the distorted one presents minor renormalization of intensities. It is striking that the d DOS of a seven-atom cluster is so close to that of a 55 atom one, in contrast to the p DOS (Sec. IV B 1). This indicates that band effects are much less effective for d states than for p states, due to their higher localization.

C. Local DOS on the oxygen atoms

We have calculated the electronic structure of O clusters and, in this section, we will discuss successively the DOS in the conduction band projected on oxygen p orbitals, in connection with the oxygen K edge, and the shape of the valence band.

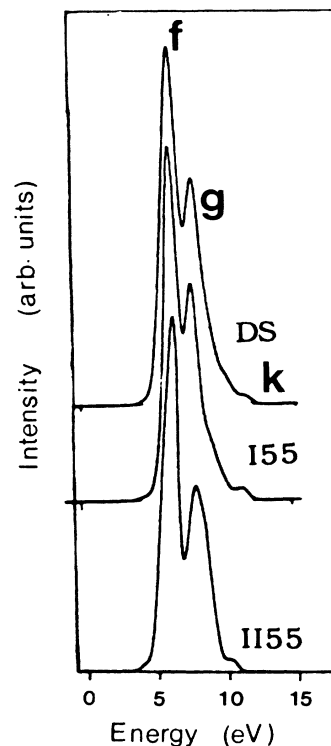


FIG. 7. d local DOS (conduction band) on type-I and type-II yttrium atoms, at the center of a 55-atom cluster (I55 and II55); mean value (DS). Peaks f and g correspond to the experimental peaks α and β of Fig. 3.

1. *K* edge

The conduction band of Y_2O_3 is mainly of yttrium character: the electrons, in this energy range, have a higher probability of presence on Y atoms than on O ones. When focusing on the local DOS on oxygen atoms, one may thus understand that its energy distribution reflects the yttrium structures (already discussed in Sec. IV B). On the other hand, in our 45 atom-O clusters, it occurs that the four yttrium atoms in the first shell do not have exactly the same environment because of finite-size effects. This difference, which would not exist in the infinite crystal, induces different Coulomb fields on these atoms, and thus produces an unphysical multiplication of Y structures, which has to be corrected.

After correction, the local DOS of *p* character has two main structures, as displayed in Fig. 9, which, from lower to higher energy, follow closely the position of the e_g and t_{1u} structures in the Y DOS. This is in fair agreement with our experimental finding, and allows us to adjust the value of the yttrium *p* orbital energy, which is not well known. A value $\epsilon_p = -2.86$ eV gives the right separation of about 5 eV. In Fig. 9, no structure corresponds to the location of the t_{2g} yttrium orbitals, likely because the lo-

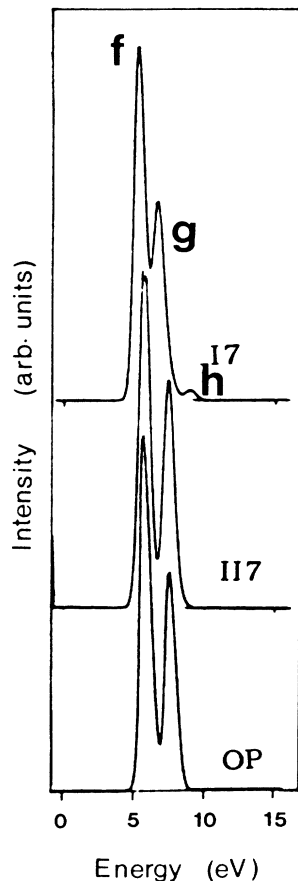


FIG. 8. *d* local DOS (conduction band) on type-I and type-II yttrium atoms, at the center of a seven-atom cluster (I7 and II7), and in a perfect octahedral environment (OP).

cal geometry imposes a hybridization between oxygen *p* orbitals and yttrium d_{xy}, d_{yz}, d_{zx} orbitals much weaker than with the d_{z^2} and $d_{x^2-y^2}$ ones. As concerns the relative intensities of the two peaks, our agreement with the data is not good but we do not think that it should lead us to reconsider the calculation. For help in understanding this point, let us recall that the experimental spectrum has been, in fact, recorded on a substoichiometric sample. Similar calculations made on substoichiometric O clusters, and that will be published elsewhere, seem to give good agreement with the relative intensities of the peaks of the experimental spectrum.

We finally comment on the similarity between the shape of the oxygen *K* edge in Y_2O_3 and in various isoelectronic oxides, such as $Sc_2O_3, La_2O_3, Gd_2O_3$, recorded by means of EELS.²³ The two peaks were said to be the signature of the tetrahedral environment of the oxygen atoms. Following the preceding discussion, we further add that the presence of *d* orbitals on the cations seems to be also a necessary condition.

2. Shape of the valence band

Figure 10 displays the local DOS on an oxygen atom in the valence band, which should be compared with the photoemission spectra (Fig. 5). Actually, the yttrium orbitals also contribute to a smaller extent to the valence band. But, considering our procedure which makes use of one type of cluster for the Y DOS and another for the

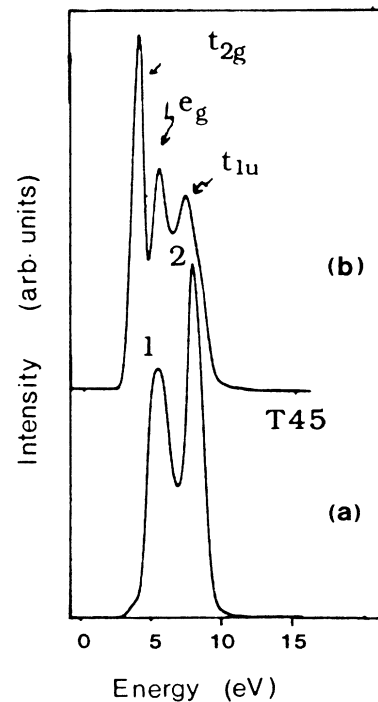


FIG. 9. (a) *p* local DOS (conduction band) on an oxygen atom at the center of a 45-atom cluster. Peaks 1 and 2 correspond to the experimental peaks *c* and *d* of Fig. 4(b). (b) Mean local DOS (conduction band) on yttrium.

O DOS, it was very difficult to find a common reference of energy. However, we have verified on the Y DOS that the contributions of the yttrium orbitals was flat in the valence band. We thus only comment on the local DOS on oxygen.

The valence band presents an intense peak, labeled *c*, and a weaker relevant one, labeled *b*. The weak features *a*, *d*, and *e* are due to finite-size effects and will be discarded. The more intense peak is the signature of *p* orbitals in a pure or distorted tetrahedral environment, while the second peak clearly comes from band effects, as may be checked on the DOS of a five-atom O cluster. In order to understand the importance of band effects, and also because, at this stage, the comparison with the three experimental peaks was not satisfactory, we have introduced in the calculation direct oxygen-oxygen hopping terms: for this, we have used the values empirically determined by Allan *et al.*²⁶ in quartz, in which the O-O distance is close to that of Y_2O_3 (2.65 Å). The result is shown in Fig. 11 and goes in the direction of a better agreement with experimental data: the relative weight of peaks *b* and *c* has changed to the benefit of *b*, which reinforces its preceding assignment to band effects. We also checked that the introduction of these hopping integrals did not modify the results obtained for the *K* edge. We were not able to further improve the shape of the valence band, more likely because the size of the O clusters remains too small, but the above discussion clearly establishes the relevance of O-O hopping terms.

D. Summary of the electronic structure of Y_2O_3

A sketch of the total DOS of Y_2O_3 is shown in Fig. 12. It was obtained by collecting the local DOS on an oxygen

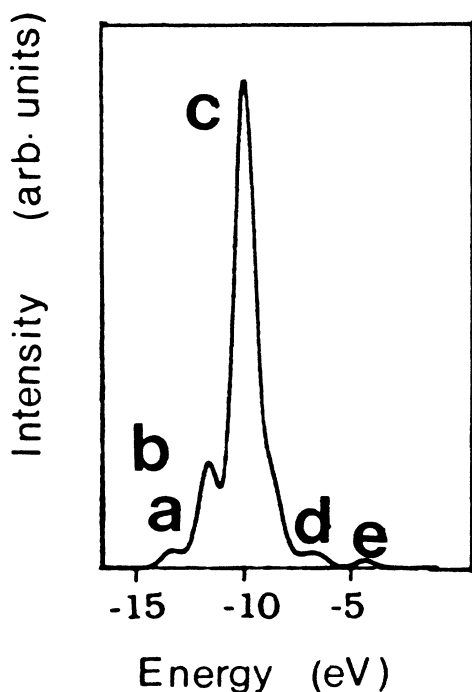


FIG. 10. Local *p* DOS (valence band) on an oxygen atom at the center of a 45-atom cluster.

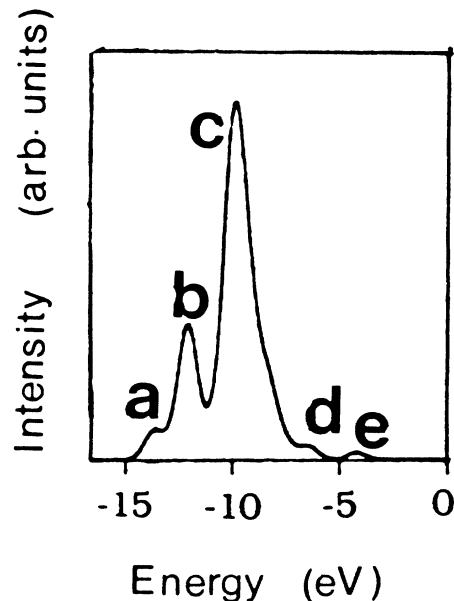


FIG. 11. Local *p* DOS (valence band) on an oxygen atom at the center of a 45-atom cluster, taking into account O-O hopping terms.

atom for the valence band (O cluster with 45 atoms) and the sum of the local DOS on yttrium atoms for the conduction band ($\frac{3}{4}$ type-I cluster + $\frac{1}{4}$ type-II cluster with 55 atoms).

Although the sizes of the clusters were not very large (45 or 55 atoms at most), the charges on the ions seem reliable. At the end of the self-consistent procedure, in the 55 atoms Y clusters, we find $Q_{YI} = 1.62$ and $Q_{YII} = 1.67$, respectively, on type-I and type-II yttrium atoms. In the 45-atom O cluster, we find $Q_O = -1.07$. Up to the precision expected in the calculation, these values are consistent since they nearly fulfill the neutrality condition:

$$Q_O = -\frac{2}{3}Q_Y \quad (Q_Y = \frac{3}{4}Q_{YI} + \frac{1}{4}Q_{YII}).$$

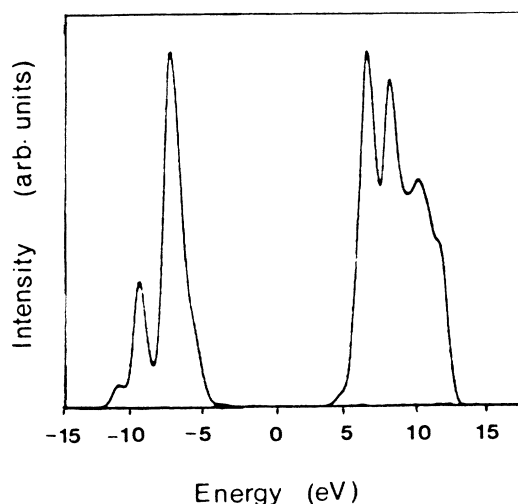


FIG. 12. A sketch of the total DOS of Y_2O_3 (see text).

V. CONCLUSION

We have studied the electronic structure of Y_2O_3 both experimentally and theoretically. By means of x-ray absorption, obtained through total-yield measurements, and photoemission spectroscopy, we have obtained information on empty states of various orbital symmetries in the conduction band, and on the shape of the valence band. We have compared them with self-consistent, semiempirical tight-binding calculations applied to clusters of increasing sizes. The most striking results are the following.

An overall knowledge of Y_2O_3 electronic structure has been obtained as represented in Fig. 12. The various calculations have given an estimate of the degree of covalency of the Y—O bond.

The quasi-octahedral local environment of the yttrium atoms is an important ingredient to understand their d local DOS, but as concerns the DOS projection on p orbitals, molecular considerations restricted to an octahedron are not adequate.

Band effects are also very important to interpret the shape of the valence band and we have shown that the introduction of direct hopping terms between neighboring oxygen atoms is necessary to account for the lower energy peak in that band.

Finally, the two-peak shape of the oxygen K edge results from the hybridization of the O p orbitals with both the e_g and the t_{1u} states on the cation.

ACKNOWLEDGMENTS

The authors are grateful to D. Chandesris, P. Lagarde, and G. Rossi for experimental assistance and advice and to the staff of LURE for providing synchrotron radiation and associated facilities. They are indebted to F. Valin and P. Bergez (DLPC-CEN, Saclay) for their help in conducting sintering and redox treatments of the sample. They thank G. Allan (Institut Supérieur d'Électronique du Nord, Lille) for providing the code allowing DOS calculations, and G. Allan, M. Lanoo, and S. Russo for fruitful discussions.

*Also at Laboratoire de Physique du Solide, 91400 Orsay, France.

¹A. A. Kaminskii, in *Laser Crystals* (Springer-Verlag, Berlin, 1981).

²M. Gurcitch, L. Manchanda, and J. M. Gibson, *Appl. Phys. Lett.* **51**, 919 (1987).

³T. Norby and P. Kofstad, *Solid State Ionics* **20**, 169 (1986).

⁴G. Fantozzi *et al.*, *J. Am. Ceram. Soc.* **72**, 1562 (1989).

⁵F. Jollet *et al.*, *J. Am. Ceram. Soc.* **71**, C396 (1988).

⁶M. Gautier *et al.*, in *Surfaces and Interfaces of Ceramic Materials*, Vol. 173 of *NATO Advanced Study Institute, Series E: Applied Sciences*, edited by L. C. Dufour (Kluwer, Dordrecht, 1989), p. 351.

⁷J. P. Duraud *et al.*, *J. Am. Ceram. Soc.* (to be published).

⁸P. Odier and J. P. Loup, *J. Solid State Chem.* **34**, 107 (1980).

⁹T. Tomiki *et al.*, *J. Phys. Soc. Jpn.* **55**, 4543 (1986).

¹⁰J. Frandon, B. Brousseau, and F. Pradal, *Phys. Status Solidi B* **98**, 379 (1980).

¹¹M. Gasgnier and L. M. Brown, *J. Microsc. Spectrosc. Electron* **10**, 437 (1985).

¹²V. N. Abramov, A. N. Ermoshkin, and A. I. Kuznetsov, *Fiz. Tverd. Tela (Leningrad)* **25**, 1703 (1983) [*Sov. Phys.—Solid State* **25**, 98 (1983)].

¹³J. Stöhr, C. Noguera, and T. Kendelewicz, *Phys. Rev. B* **30**, 5571 (1984).

¹⁴A. P. Lukirskii and I. A. Britov, *Fiz. Tverd. Tela (Leningrad)* **6**, 43 (1964) [*Sov. Phys.—Solid State* **6**, 33 (1964)].

¹⁵A. P. Lukirskii, O. A. Ershov, T. M. Zimkina, and E. P. Savinov, *Fiz. Tverd. Tela (Leningrad)* **8**, 1787 (1966) [*Sov. Phys.—Solid State* **8**, 1422 (1966)].

¹⁶W. Gudat and C. Kunz, *Phys. Rev. Lett.* **29**, 169 (1972).

¹⁷J. P. Vigouroux *et al.*, *J. Appl. Phys.* **57**, 5139 (1985).

¹⁸R. D. Leapman, L. A. Grunes, and P. L. Frejles, *Phys. Rev. B* **26**, 614 (1982).

¹⁹J. A. Bearden, in *X-Ray Atomic Energy Levels*, Natl. Bur. Stand. Ref. Data Ser., Natl. Bur. Stand. (U.S.) Circ. No. 14 (U.S. GPO, Washington, D.C., 1967).

²⁰A. Fujimori and L. Schlapbach, *J. Phys. C* **17**, 341 (1986).

²¹C. D. Wagner, *J. Electron Spectrosc. Relat. Phenom.* **10**, 305 (1977).

²²K. D. Sevier, *Low Energy Electron Spectrometry* (Wiley Interscience, New York, 1972), p. 228.

²³C. Colliex, T. Manoubi, M. Gasgnier, and L. M. Brown, *Scanning Electron Microscopy II*, edited by Om Jahari (Scanning Electron Microscopy, Chicago, 1985), p. 489.

²⁴W. A. Harrison, *Electronic Structure and Properties of Solids* (Freeman, San Francisco, 1980); W. A. Harrison, *Phys. Rev. B* **24**, 5835 (1981); **31**, 2121 (1985).

²⁵See, e.g., J. C. Chadi, *Phys. Rev. B* **29**, 785 (1984); J. A. Majewski and P. Vogl, *Phys. Rev. Lett.* **57**, 1366 (1986); I. Lefebvre, M. Lanoo, G. Allan, and L. Martinage, *Phys. Rev. B* **38**, 8593 (1988).

²⁶G. Allan and M. Lanoo, *J. Phys. (Paris)* **44**, 1355 (1983).